Magnetoelasticity of dilute Cr - Ir alloy single crystals

1997 J. Phys.: Condens. Matter 9 3461

(http://iopscience.iop.org/0953-8984/9/16/017)

J. Phys.: Condens. Matter **9** (1997) 3461–3478. Printed in the UK PII: S0953-8984(97)81357-4

Magnetoelasticity of dilute Cr–Ir alloy single crystals

J Martynova, H L Alberts and P Smit

Department of Physics, Rand Afrikaans University, PO Box 524, Auckland Park, Johannesburg 2006, South Africa

Received 28 January 1997

Abstract. Measurements are reported of the temperature dependence of the elastic constants, ultrasonic attenuation and thermal expansion of dilute Cr–Ir alloy single crystals containing 0.07, 0.17, 0.20 and 0.25 at.% Ir. Well defined magnetic anomalies were observed in the elastic constants and in the thermal expansion at the Néel points (T_N) and at the incommensurate–commensurate (I–C) spin-density-wave (SDW) transition temperatures (T_{IC}). The transition at T_{IC}, observed in Cr + 0.20 at.% Ir and Cr + 0.25 at.% Ir, is hysteretic, of hysteresis width about 20 K. Magnetic anomalies were also observed in the elastic constants at the spin-flip transition temperature (T_{sf}), The attenuation coefficient (γ) shows a large spike-like peak at T_{IC} (on heating) and at T_{CI} (on cooling) for Cr + 0.20 at.% Ir. These peaks are however smeared out by inhomogeneities in the crystal containing 0.25 at.% Ir. The attenuation coefficient peaks at T_{sf} and T_N in Cr + 0.07 at.% Ir and in Cr + 0.17 at.% Ir. Due to very large attenuation and the high value of T_N, γ could not be measured successfully around the Néel point for the other crystals. The magnetovolume ($\Delta\omega$) and magnetic contributions (ΔB) to the bulk modulus (B) have been found to fit the equation $a + bT^2 + cT^4$, predicted by theory, rather well up to temperatures (T) close to T_N. The volume derivative of T_N calculated from $\Delta\omega$ and ΔB for Cr + 0.07 at.% Ir, compares fairly well with the value obtained from high-pressure measurements. High-pressure measurements are not available for the other crystals for a similar comparison. The temperature dependence of γ for Cr + 0.17 at.% Ir fits the power law $(T/T_N - 1)^{-5/4}$, predicted by theory for T just above T_N, rather well. The theory however fails in the case of Cr + 0.07 at.% Ir and could not be tested for the other two crystals.

1. Introduction

Spin-density-wave (SDW) effects in dilute Cr alloys with group-8 non-magnetic transition metals Ru, Os, Rh, Ir and Pt are of interest and are receiving attention in the literature [1–4]. Their magnetoelastic properties are of particular interest. The interest in these properties arises from the relatively large components contributed by the SDW to the elastic constants and volume of the alloys.

Four magnetic phases appear [1] on the magnetic phase diagram of dilute Cr alloys with group-8 non-magnetic transition metals. The magnetic phase diagram contains a triple-point concentration, c_t, where three phases coexist; the incommensurate (I) SDW, the commensurate (C) SDW and the paramagnetic (P) phases. For $c > c_t$ the alloys have three possible magnetic phase transitions. These are the I–C and C–P transitions, occurring respectively at the temperature T_{IC} and at the Néel temperature T_N, $T_{IC} < T_N$, as well as the spin-flip transition at the temperature $T_{sf} < T_{IC}$, where the transverse (T) ISDW phase above T_{sf} transforms to a longitudinal (L) ISDW phase below T_{sf}. For $c < c_t$ there is no I–C transition, the alloy remains in the ISDW phase at all $T < T_N$, and only two phase transitions are possible, an I–P one at T_N and a TISDW–LISDW one at $T_{sf} < T_N$.

0953-8984/97/163461+18$19.50

Most existing magnetoelastic studies on dilute Cr alloys with group-8 non-magnetic transition metals were done on polycrystalline material and were reported for Cr–Pt [4], Cr–Ru [5, 6], Cr–Ir [3] and Cr–Rh [5] alloys. These studies show interesting behaviour in the temperature dependence of the elastic constants, the bulk modulus (B) and shear modulus (G), or in the Young's modulus, and in the case of Cr–Pt and Cr–Ir also of the magnetovolume, when these alloys are taken through the above-described magnetic phase transition temperatures. Unfortunately the magnetovolume has been reported up to now only for Cr–Pt and Cr–Ir polycrystalline alloys and one does not know whether similar interesting behaviour—a sharp and large maximum in α–T at T_{IC}, where α is the coefficient of thermal expansion, and a sharp and large minimum at T_N due to the effects of the SDW—is also characteristic of the other alloy systems mentioned above. The B–T curves of polycrystalline Cr–Pt [4], Cr–Ru [6] and Cr–Ir [3] show large minima at T_N, as is also observed for Young's modulus for Cr–Rh [5]. The B–T behaviour at T_{IC} is however different. It shows a relatively large step-like decrease in B when Cr–Ru and Cr–Ir are heated through T_{IC} (and also in Young's modulus for Cr–Rh), but this anomaly is absent for Cr–Pt alloys [4]. G on the other hand shows relatively small anomalies near both T_{IC} and T_N for Cr–Ru and Cr–Ir alloys but none, neither at T_{IC} nor at T_N, for Cr–Pt alloys. G has not been studied for Cr–Rh alloys yet. The other interesting aspect of the previous studies is the large hysteresis, of width about 20 K, observed in the B–T and G–T curves of a polycrystalline Cr + 0.25 at.% Ir alloy.

Measurements on polycrystalline material are of limited value, particularly elastic constant measurements, and measurements on single-crystalline alloys are needed for a better understanding of the observed phenomena. Only three single crystals in the above group of alloys have been studied up to now. These are single crystals of Cr + 0.3 at.% Ru, Cr + 0.5 at.% Ru and Cr + 0.20 at.% Ir for which all of the independent elastic stiffness tensor components c_{11}, $c' = \frac{1}{2}(c_{11} - c_{12})$ and c_{44} have been measured [7–10]. Thermal expansion measurements of these alloy single crystals have however not been reported yet.

In order to investigate the Cr alloy system with group-8 non-magnetic transition metals further, we report here a comprehensive study of the elasticity and magnetovolume of four Cr–Ir alloy single crystals, two with $c > c_t$, one with $c < c_t$ and one with c close to c_t.

2. Experimental details

Four Cr–Ir alloy single crystals, containing 0.07, 0.17, 0.20 and 0.25 at.% Ir, were grown by a floating-zone technique using RF heating in a pure argon atmosphere as previously described [11]. The starting materials were 99.996% pure Cr and 99.9% pure Ir. Ir is soluble in Cr up to about 12 at.% at 1680 °C [12]. The actual concentrations of 0.07 at.% Ir, 0.17 at.% Ir, 0.20 at.% Ir and 0.25 at.% Ir were determined using electron microprobe analyses techniques. The error in the absolute value of these concentrations is about 20 to 25%. The error is fairly large due to the low concentrations involved. The crystals were prepared with a pair of flat and parallel (110) faces and for some crystals also with flat and parallel (100) faces. The distance between these parallel faces was about 6 mm and the area of the flat surface about 30 mm^2. The elastic constants c_{11}, $c' = \frac{1}{2}(c_{11} - c_{12})$, c_{44} and $c_L = \frac{1}{2}(c_{11} + c_{12} + 2c_{44}$ were determined from measurements of ultrasonic wave velocities propagating along the [110] and [100] directions. Standard phase-comparison [13] and pulse–echo overlap techniques [14] were used to determine ultrasonic (10 MHz) wave velocities. The sensitivity of the former technique is 1 part in 10^3 or better, and that of the latter about 1 part in 10^5. The error in the absolute values of the ultrasonic

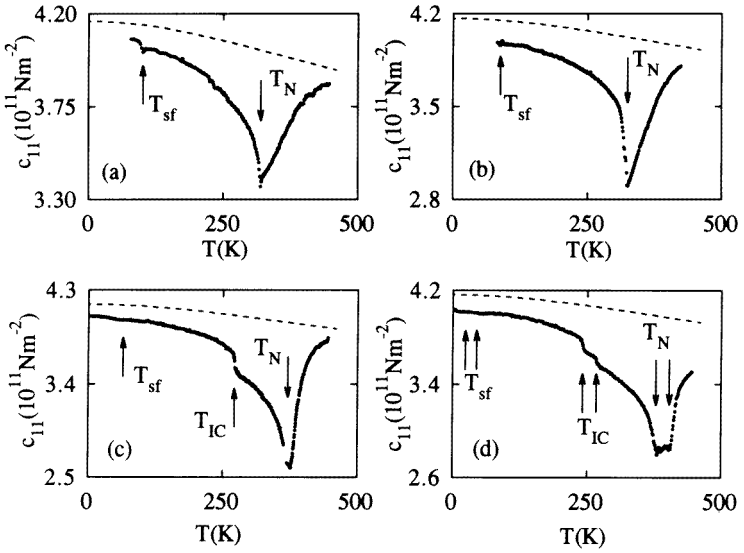

Figure 1. The temperature dependence (on heating) of the elastic constant c_{11} for (a) Cr + 0.07 at.% Ir, (b) Cr + 0.17 at.% Ir, (c) Cr + 0.20 at.% Ir and (d) Cr + 0.25 at.% Ir. The broken curves are the expected non-magnetic behaviour determined from the results for Cr + 5 at.% V [18].

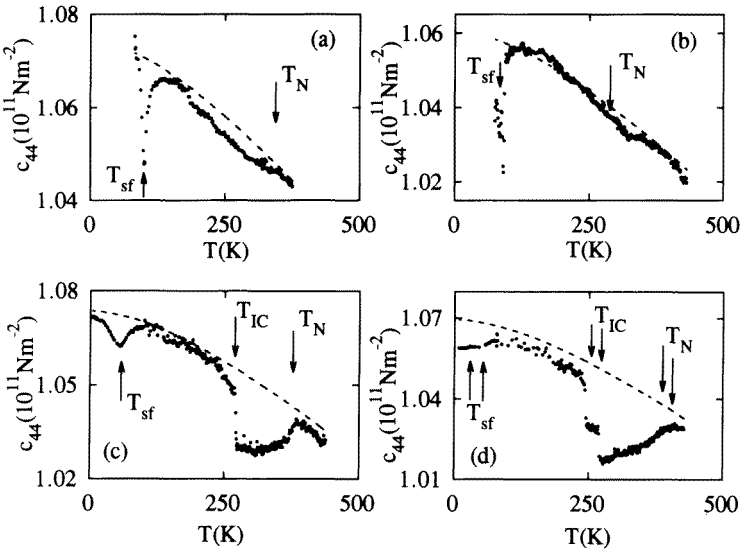

Figure 2. The temperature dependence of the elastic constant c_{44} for (a) Cr + 0.07 at.% Ir, (b) Cr + 0.17 at.% Ir, (c) Cr + 0.20 at.% Ir and (d) Cr + 0.25 at.% Ir. The broken curves are the expected non-magnetic behaviour determined from the results for Cr + 5 at.% V [18].

wave velocities is about 0.5 to 1.0%. The phase-comparison technique was more useful for measurements over a wide temperature range where the changes in ultrasonic wave velocities with temperature are large, while the pulse–echo overlap technique was useful for the studies around the phase transition temperatures and for measuring ultrasonic wave

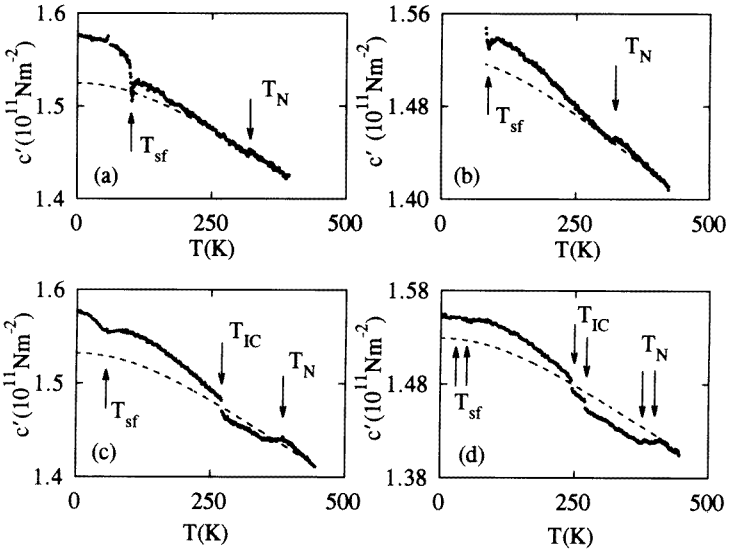

Figure 3. The temperature dependence of the elastic constant $c' = \frac{1}{2}(c_{11} - c_{12})$ for (a) Cr+0.07 at.% Ir, (b) Cr+0.17 at.% Ir, (c) Cr+0.20 at.% Ir and (d) Cr+0.25 at.% Ir. The broken curves are the expected non-magnetic behaviour determined from the results for Cr + 5 at.% V [18].

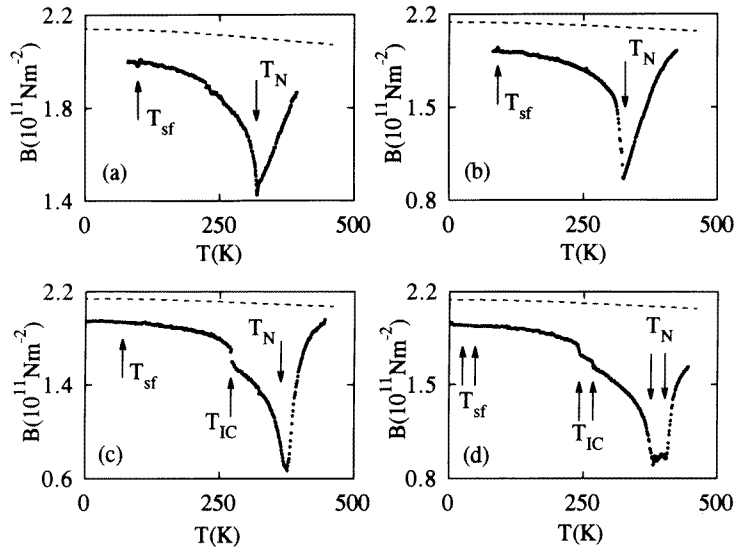

Figure 4. The temperature dependence of the bulk modulus $B = \frac{1}{3}(c_{11} + 2c_{12})$ for (a) Cr+0.07 at.% Ir, (b) Cr+0.17 at.% Ir, (c) Cr+0.20 at.% Ir and (d) Cr+0.25 at.% Ir. The broken curves are the expected non-magnetic behaviour determined from the results for Cr + 5 at.% V [18].

attenuation near these temperatures.

Thermal expansion measurements were made using a strain gauge technique. These measurements were done relative to Cr + 5 at.% V, which remains paramagnetic at all temperatures and serves [1, 15] to simulate the non-magnetic component of the Cr–Ir

Table 1. The magnetic transition temperatures T_{sf}, T_{IC}, T_{CI} and T_N for Cr–Ir alloys obtained from thermal expansion, velocity of sound, ultrasonic attenuation and electrical resistivity measurements.

at.% Ir	Transition temperature (K)	From thermal expansion	From ultrasonic velocity	From ultrasonic attenuation	From resistivity measurements
0.07	T_{sf}	—	101.1 ± 0.9	100 ± 2	—
	T_N	318 ± 1	320.0 ± 0.4	320.5 ± 0.6	317 ± 4
0.17	T_{sf}	—	86.1 ± 0.4	84 ± 3	—
	T_N	322 ± 1	323.9 ± 0.4	322.1 ± 0.2	324 ± 9
0.20	T_{sf}	—	58 ± 2	—	—
	T_{IC}	270 ± 1	272 ± 1	272.3 ± 0.2	273 ± 3
	T_{CI}	254 ± 1	255 ± 1	255.7 ± 0.1	255 ± 3
	T_N	385 ± 5	376 ± 1	—	378 ± 1
0.21	T_{sf}	—	53 ± 6	—	—
	T_{IC}	—	270 ± 2	—	—
	T_{CI}	—	248 ± 3	—	—
	T_N	—	380 ± 4	—	—
0.25	T_{sf}	—	22 ± 6	—	—
	T_{IC}	258 ± 3	245 ± 2	—	—
	T_{CI}	235 ± 5	214 ± 4	—	—
	T_N	389 ± 5	402 ± 8	—	391.5 ± 0.5

crystals, i.e. $(\Delta L/L)_{meas} = (\Delta L/L)_{\mathrm{Cr-V}} - (\Delta L/L)_{\mathrm{Cr-Ir}}$. The error in the absolute values of $\Delta L/L$ is about 5%, while changes of 3×10^{-7} could be detected easily. Measurements for thermal expansion were recorded at 0.1 K intervals while slowly heating or cooling the samples at a rate of about 0.3 K min^{-1}. The heating and cooling rates for the ultrasonic measurements were about 0.5 K min^{-1}.

3. Results

3.1. Ultrasonic measurements

The elastic constants were obtained from the ultrasonic wave velocities and densities of the crystals by using the standard equations [16] for cubic crystals. Densities were determined by hydrostatic weighing in water. Ultrasonic wave velocity data were corrected for transducer diffraction effects by using methods developed by Kittinger [17]. The elastic constants were corrected for the effects of thermal expansion of the sample by using the thermal expansion measurements reported in the next section. Wave velocity measurements were done in the temperature range from liquid nitrogen or liquid helium temperatures up to 450 K.

The temperature dependences of c_{11}, c_{44}, $c' = \frac{1}{2}(c_{11} - c_{12})$ and of the bulk modulus $B = \frac{1}{3}(c_{11} + 2c_{12})$ are shown, respectively, in figures 1, 2, 3 and 4. Also shown in these figures are the temperature dependences of the same quantities for a Cr + 5 at.% V alloy single crystal [18]. This latter crystal remains paramagnetic for all $T > 0$ K and the temperature dependences of its elastic constants represent [1, 15] that of the non-magnetic

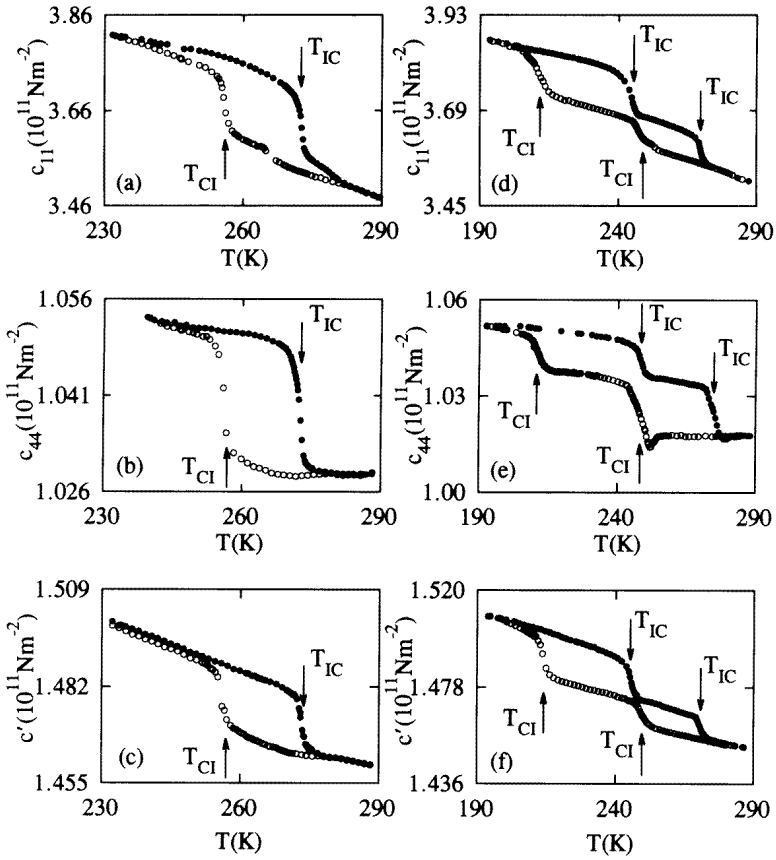

Figure 5. The temperature dependences of c_{11}, c_{44} and $c' = \frac{1}{2}(c_{11} - c_{12})$ of Cr + 0.20 at.% Ir (panels (a), (b) and (c)) and of Cr + 0.25 at.% Ir (panels (d), (e) and (f)) near the I–C and C–I phase transition temperatures. Points marked ● were measured during heating runs and those marked ○ were measured during cooling runs.

component of the corresponding elastic constant for a Cr–Ir alloy.

The longitudinal mode elastic constant c_{11} as well as B show deep minima of magnetic origin at T_N and step-like decreases at T_{IC} on heating. The transition at T_{IC} shows a large hysteresis effect in all elastic constants on heating and cooling, as shown in figure 5 for the two crystals containing respectively 0.20 and 0.25 at.% Ir. The width of the hysteresis for the 0.20 at.% Ir alloy is about 20 K. For the 0.25 at.% Ir alloy the transition at T_{IC} (on heating) and at T_{CI} (on cooling) each appear in two steps (figure 5) while the transition at T_N seems to be smeared out (figures 1 and 4). This is probably due to sample inhomogeneities in this crystal. In fact, electron microprobe analyses at up to about 100 points on the surface of the two crystals containing 0.20 and 0.25 at.% Ir show that the former crystal is of much better homogeneity than the latter. The 0.25 at.% Ir crystal was found to have a distinctive part with a fraction of roughly one third of the surface through which the average concentration, 0.21 at.% Ir, was about 16% lower than for the rest (0.25 at.% Ir) of the crystal. X-ray Laue diffraction photos on these two parts show that they are in the same crystal. We nevertheless show the results for the Cr + 0.25 at.% Ir crystal, as it clearly shows the type of magnetic anomalies observed at T_{sf}, T_{IC} and T_N. The results for

this crystal corroborate the general form of the anomalies observed at these temperatures for the elastic constants of the Cr + 0.20 at.% Ir sample, which is of good homogeneity.

T_N was taken at the deep minima on the c_{11}–T curves of figure 1. The values of T_N obtained in this way are also shown in figures 2, 3 and 4 which show the type of anomalies observed in c_{44}, c' and B at T_N. T_{IC} (on heating) and T_{CI} (on cooling) were taken at the inflection points of the sharp steps in figure 5. For the Cr + 0.20 at.% Ir alloy we obtained $T_{IC} = 272 \pm 1$ K and $T_{CI} = 255 \pm 1$ K which corresponds very well with values obtained from electrical resistivity measurements [19] on a sample cut from the same crystal boule. Electrical resistivity studies give $T_{IC} = 273 \pm 3$ K and $T_{CI} = 255 \pm 3$ K. The results suggest a first-order magnetic ISDW–CSDW transition in Cr–Ir single crystals as was previously also observed [8, 9] for a Cr+0.3 at.% Ru alloy single crystal. The ISDW–CSDW transition in the Cr + 0.25 at.% Ir alloy occurs in two distinctive steps (figure 5) characterizing the two distinct regions of the different concentrations in this crystal. We interpret one step as occurring for the part of the crystal of concentration 0.21 at.% Ir and the other step for the rest of the crystal with concentration 0.25 at.% Ir. The temperatures T_{IC} and T_{CI} at each of these steps fit well into the Cr–Ir magnetic phase diagram [19, 20]. This is also the case for T_N estimated from figure 1(d) for the two parts of the crystal.

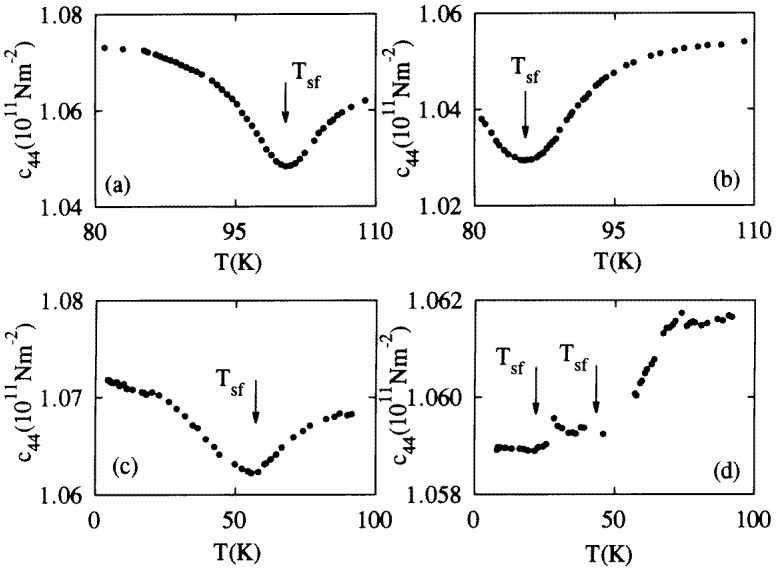

Figure 6. The temperature dependence of c_{44} near the spin-flip transition temperature for (a) Cr + 0.07 at.% Ir, (b) Cr + 0.17 at.% Ir, (c) Cr + 0.2 at.% Ir and (d) Cr + 0.25 at.% Ir. Note the different temperature scales of the different panels.

The magnetic anomalies at the spin-flip transition temperature, T_{sf}, are most clearly observed in the shear elastic constants c_{44} and c' of figures 2 and 3. An example of the behaviour close to T_{sf} is shown in figure 6 for c_{44} for the four crystals. No hystereses were observed between heating and cooling runs through T_{sf}. T_{sf} was defined at the minimum points shown in this figure. Table 1 gives the transition temperatures obtained in this study from ultrasonic and thermal expansion measurements. Also given in table 1 are values deduced for 0.21 at.% Ir from the distinctive behaviour of the two parts of the 0.25 at.% Ir alloy. The transition temperatures of these two parts fit in rather well with the data for the

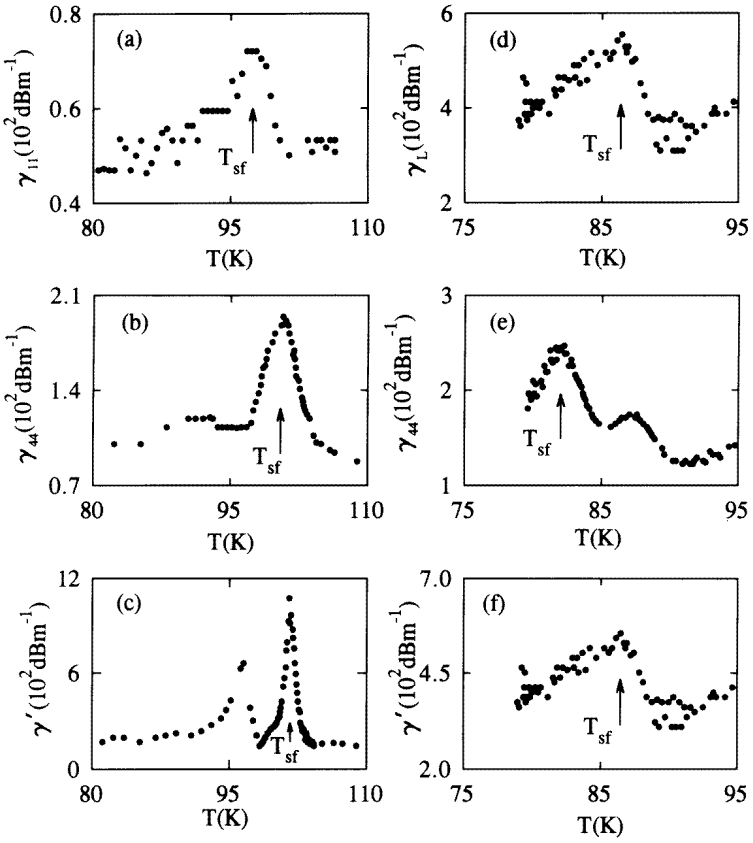

Figure 7. Ultrasonic attenuation coefficients, γ, for the c_{11}, c_{44}, $c_L = \frac{1}{2}(c_{11} + c_{12} + 2c_{44})$ and $c' = \frac{1}{2}(c_{11} - c_{12})$ mode wave propagations as functions of temperature near the spin-flip transition temperature. Panels (a), (b) and (c) are for Cr + 0.07 at.% Ir and panels (d), (e) and (f) for Cr + 0.17 at.% Ir.

other samples. T_N and T_{IC} for this study correspond well with values obtained in previous studies [19, 20] on Cr–Ir alloys using different techniques. T_{sf} was however not previously determined.

The ultrasonic attenuation coefficient, γ, for the c_{11}, c_{44}, c_L and c' propagation modes near the spin-flip transition temperature is shown in figure 7 for the Cr–Ir crystals containing 0.07 and 0.17 at.% Ir. This quantity was not studied for the crystals containing 0.20 and 0.25 at.% Ir. γ shows well defined peaks at T_{sf} for Cr + 0.07 at.% Ir and Cr + 0.17 at.% Ir. The temperatures of these peaks agree well with the temperatures of the small minima in c_{44} near T_{sf} (figure 6 and table 1). No hysteresis effects were observed, within the experimental error in γ near T_{sf} for the crystals containing 0.07 and 0.17 at.% Ir. Another Cr alloy in which γ was previously measured is a Cr + 0.5 at.% V single crystal for which γ was measured [21] for longitudinal sound propagation only, in both the poly-$\boldsymbol{Q}$ and single-$\boldsymbol{Q}$ states. Our crystals were not field cooled and are therefore in the poly-$\boldsymbol{Q}$ state. For Cr + 0.5 at.% V in the poly-$\boldsymbol{Q}$ state, γ for longitudinal modes shows [21] a small step-like decrease when the TISDW phase is entered with increasing temperature through T_{sf}. This is to be compared with peaks observed at T_{sf} in γ for all three propagation modes of poly-$\boldsymbol{Q}$

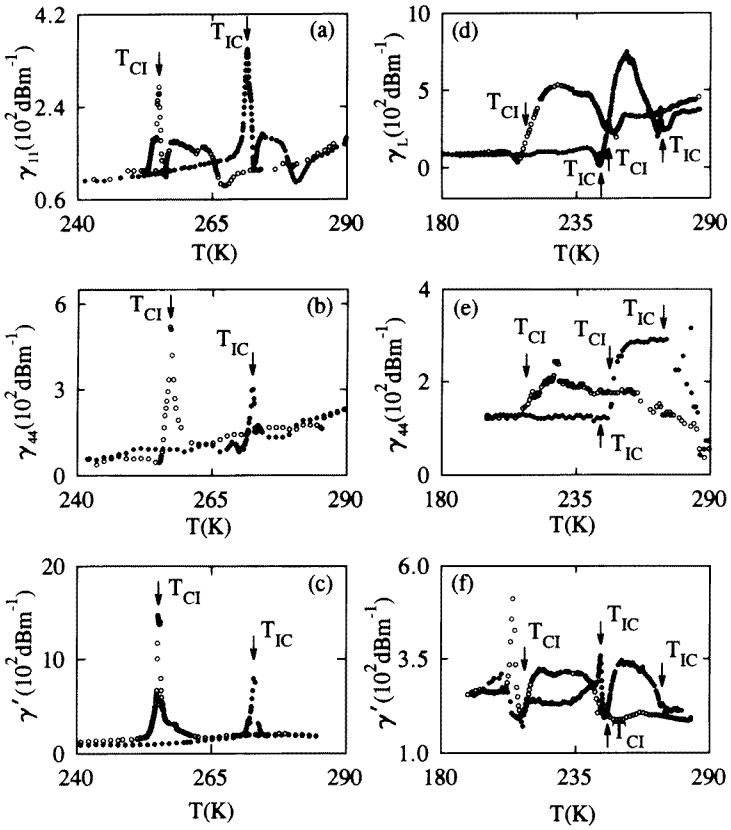

Figure 8. Ultrasonic attenuation coefficients, γ, for the c_{11}, c_{44}, $c_L = \frac{1}{2}(c_{11} + c_{12} + 2c_{44})$ and $c' = \frac{1}{2}(c_{11} - c_{12})$ mode wave propagations as functions of temperature near the I–C (on heating, points ●) and C–I (on cooling, points ○) phase transition temperatures. Panels (a), (b) and (c) are for Cr + 0.20 at.% Ir and panels (d), (e) and (f) for Cr + 0.25 at.% Ir. Temperatures T_{CI} and T_{IC} marked in panels (d), (e) and (f) for the Cr + 0.25 at.% crystal are values taken from figures 5(d), 5(e) and 5(f). For Cr + 0.20 at.% Ir, T_{IC} and T_{CI} marked at the peaks in panels (a), (b) and (c) in this figure correspond closely to the same temperatures marked for the same crystal in figure 5. Note that in panels (d), (e) and (f) there are two values of T_{IC} and T_{CI} for each panel. These are due to the two distinct parts of different concentrations in the crystal containing 0.25 at.% Ir used in the ultrasonic work. In each of panels (d), (e) and (f) the two T_{IC}-values marked refer to the heating curves (●) and those marked T_{CI} to the cooling curves (○).

Cr + 0.07 at.% Ir and Cr + 0.17 at.% Ir alloys of the present study.

Figure 8 shows γ for the c_{11}, c_L, c_{44} and c' modes near T_{IC} and T_{CI} for the two crystals containing 0.20 and 0.25 at.% Ir. For Cr + 0.20 at.% Ir there appear sharp peaks at T_{IC} and at T_{CI} for all of the propagation modes, similarly to those observed [8] for a Cr + 0.3 at.% Ru crystal. An interesting feature in figure 8 is the broad hump in γ just above the sharp peak observed in the c_{11} propagation mode for Cr + 0.20 at.% Ir, during both heating and cooling runs. It is rather small for the two shear modes (figure 8). The reason for this hump is suggested to be the possibility that ISDW and CSDW antiferromagnetic domains coexist near the I–C or C–I transitions, as was also suggested to be the case for a Cr + 0.3 at.% Ru crystal [8, 22]. For the Cr + 0.25 at.% Ir crystal, γ near T_{IC} and T_{CI} is smeared

out (figure 8), probably due to the inhomogeneity of the crystal.

We were not successful in measuring the ultrasonic attenuation for all modes of all of the Cr–Ir crystals near T_N. We had some success only for the two crystals containing 0.07 and 0.17 at.% Ir for which γ could only be measured successfully for the c_{11} and c' modes of the Cr + 0.07 at.% Ir crystal and for the c_{44} and c' modes of the Cr + 0.17 at.% Ir crystal. The ultrasonic attenuation for longitudinal waves in the three crystals containing 0.17, 0.20 and 0.25 at.% Ir becomes so large near and above T_N that γ for these modes falls outside the range of the equipment, making measurements of γ impossible. We also were not able to measure γ for shear mode propagation near T_N for these two crystals.

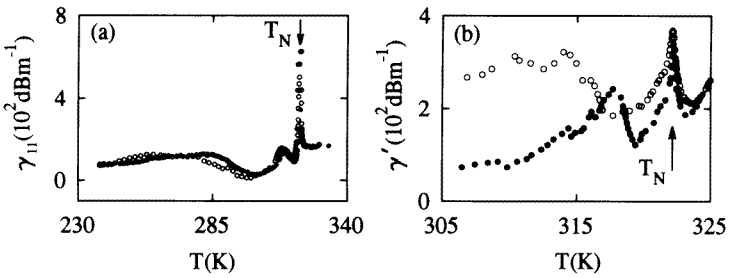

Figure 9. The ultrasonic attenuation coefficient, γ, as a function of temperature through the Néel point T_N. γ_{11} is for the c_{11} mode propagation direction of Cr + 0.07 at.% Ir (panel (a)) and γ' for the $c' = \frac{1}{2}(c_{11} - c_{12})$ mode propagation direction of Cr + 0.17 at.% Ir (panel (b)). Points marked ● were measured during heating runs and those marked ○ were measured during cooling runs. Note the different temperature scales of the two figures.

Figure 9(a) shows γ for the c_{11} propagation mode of the Cr + 0.07 at.% Ir crystal as a function of temperature. There is a very sharp and huge peak in γ at T_N, showing no hysteresis effect in the value of T_N in heating and cooling runs. An interesting observation is the small peak in the γ–T curve just below T_N. The appearance of this small peak is dependent on the thermal history of the sample and is not always present when the sample is cycled through T_N, although the peak at T_N remains unchanged during heating and cooling cycles. We think that the small peak originates from antiferromagnetic domain effects, the distribution of which depends on the thermal history of the sample.

Figure 9(b) shows the γ–T curve for the c' mode propagation of the Cr + 0.17 at.% Ir crystal. There is a small peak at T_N with a smaller peak just below T_N. The presence or absence of the latter depends on the thermal history of the sample and may also be due to antiferromagnetic domain effects. The concentration in this crystal is also very close to the triple-point concentration, meaning that the slightest sample inhomogeneities may result in parts of the crystal being in the CSDW phase and others in the ISDW phase close to and below T_N. We could not find any evidence for an I–C transition in this crystal, but the last-mentioned effect may probably also contribute to the difference in behaviour observed below T_N in figure 9(b) between heating and cooling runs. This will probably also contribute to the broadness of the T_N transition in Cr + 0.17 at.% Ir compared to that in Cr + 0.07 at.% Ir as shown in figure 10, which shows the temperature dependence of the longitudinal elastic constants c_L and c_{11}, respectively, for these two crystals close to T_N. The hysteresis below T_N for these two crystals (figure 10) is ascribed to antiferromagnetic domain effects, giving different domain patterns during heating and cooling runs [23]. No hysteresis effects were observed within the experimental error in the longitudinal mode elastic constants below T_N for the Cr + 0.2 at.% Ir and Cr + 0.25 at.% Ir crystals.

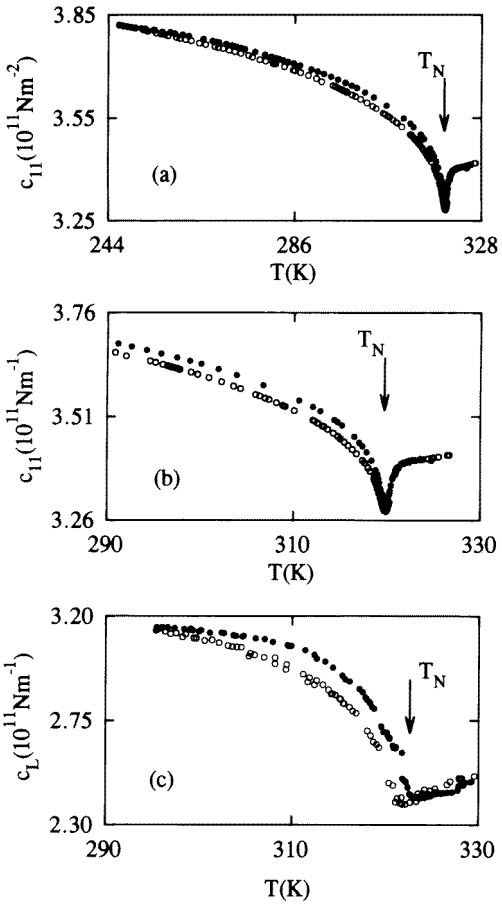

Figure 10. (a) The temperature dependence of c_{11} for Cr + 0.07 at.% Ir showing the hysteresis effects below T_N. (b) The temperature dependence of c_{11} for Cr + 0.07 at.% Ir close to T_N. Panel (b) is an enlargement of the data in (a) around T_N. (c) Hysteresis effects for $c_L = \frac{1}{2}(c_{11} + c_{12} + 2c_{44})$ for Cr + 0.17 at.% Ir near T_N. Points marked ● in these figures were measured during heating runs and those marked ○ were measured during cooling runs. Note the different temperature scales used for the different figures.

3.2. Thermal expansion

Figure 11 shows the absolute value, $|\Delta\omega|$, of the magnetovolume, $\Delta\omega$, where

$$\Delta\omega = 3(\Delta L/L)_{meas} = 3\left[(\Delta L/L)_{\mathrm{Cr-V}} - (\Delta L/L)_{\mathrm{Cr-Ir}}\right]$$

of section 2, as a function of temperature for the four Cr–Ir crystals for both heating and cooling runs. The magnetovolume of the Cr–Ir crystals is negative. An interesting point in figure 11 is the hysteresis below T_N for Cr + 0.07 at.% Ir and Cr + 0.17 at.% Ir as well as the hysteresis below T_{IC} for Cr + 0.20 at.% Ir and Cr + 0.25 at.% Ir. For the latter two crystals there are no hystereses between T_{IC} and T_N. The hysteresis effects are ascribed to antiferromagnetic domain effects. In fact similar hysteresis effects, due to the temperature dependence of the magnetic domain structure, were also observed in neutron diffraction studies below T_N of pure Cr [24] which is in the ISDW phase for all $T < T_N$ as is the case

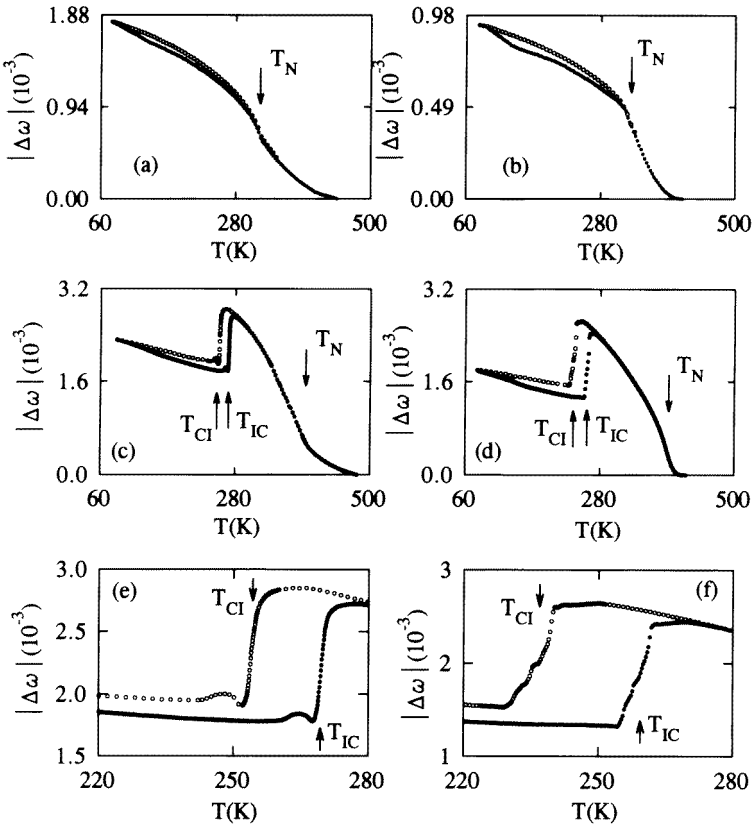

Figure 11. The absolute value, $|\Delta\omega|$, of the magnetovolume, $\Delta\omega$, as a function of temperature for (a) Cr + 0.07 at.% Ir, (b) Cr + 0.17 at.% Ir, (c) Cr + 0.20 at.% Ir and (d) Cr + 0.25 at.% Ir. Panels (e) and (f) show the behaviour close to T_{IC} and T_{CI}, respectively, for Cr + 0.20 at.% Ir and Cr + 0.25 at.% Ir. Points marked ● in these figures were measured during heating runs and those marked ○ were measured during cooling runs. Note the different temperature scales used for the different figures.

for Cr + 0.07 at.% Ir and Cr + 0.17 at.% Ir. It is interesting to note that thermal hysteresis effects persist for $\Delta\omega$ in the TISDW phases of all of the crystals (figure 11) to much lower temperatures than for γ and c_{ij} (figures 8 and 10). Hysteresis effects were also observed in the elastic constants of a Cr + 0.3 at.% Ru crystal below T_{IC} [8]. Pure Cr shows no I–C phase transition and remains in the ISDW phase below T_N. One thus expects similar thermal expansion behaviour for pure Cr and for the two Cr–Ir crystals containing 0.07 and 0.17 at.% Ir (figures 11(a) and 11(b)). We therefore also measured for comparison the thermal expansion of a pure Cr single crystal but were unable to detect any thermal hysteresis for this crystal below T_N. Two other Cr alloys that show thermal expansion hysteresis effects are polycrystals of Cr+0.55 at.% Re [25], Cr+0.6 at.% Mn and Cr+0.9 at.% Mn [26]. For these polycrystals thermal hysteresis occurs only in the temperature range of the I–C and C–I phase transitions. It does not extend to temperatures well below these phase transition temperatures as was observed in our study on the Cr–Ir alloy single crystals (figure 11). A further point of interest is that those Cr–Re and Cr–Mn alloys which do not contain an I–C transition show [25, 26] no thermal expansion hysteresis below T_N in contrast with

the observation for the Cr–Ir crystals of figures 11(a) and 11(b). As can be seen from the $|\Delta\omega|$–T curve for the Cr + 0.25 at.% Ir crystal (figure 11(f)), the inhomogeneities in this crystal only broaden the I–C and C–I transitions without showing two distinctive steps for the two crystal parts as was observed in the elastic constant measurements of figure 5.

The coefficient of thermal expansion, α, was calculated for each crystal from the $(\Delta L/L)_{meas}$–T measurements using the data of Roberts *et al* [27] for α for Cr + 5 at.% V to obtain α for the Cr–Ir crystals. The results are shown in figure 12 for heating runs. Of interest are: (i) the sharp minima in α–T at T_N for the Cr + 0.07 at.% Ir and Cr + 0.17 at.% Ir crystals, (ii) shallower, and overall broader, minima at T_N for Cr + 0.20 at.% Ir and Cr + 0.25 at.% Ir, (iii) negative or near-zero values of α near T_N for the latter two crystals, (iv) extremely large (up to about $+120 \times 10^{-6}$ K^{-1}) α-values at T_{IC} for Cr + 0.20 at.% Ir and Cr + 0.25 at.% Ir and (v) a negative magnetic contribution to α at T_N and an extremely large positive magnetic contribution to α at T_{IC} for all of the crystals. The magnetic contributions to α are given in figure 12 by the difference between the α-value for Cr + 5 at.% V (broken lines) and the measured value for the particular Cr–Ir alloy at each temperature.

4. Discussion

We used a thermodynamic model that was previously successfully used for several Cr alloys [1, 11, 28–30] to analyse the magnetic contributions to the bulk modulus and to the magnetovolume. The main assumptions of the model are that the magnetic free energy is separable from the total free energy and that volume strain terms in the free energy dominate shear strain effects. The last assumption is nearly fully satisfied for the TISDW phases of the Cr + 0.07 at.% Ir and Cr + 0.17 at.% Ir crystals for which magnetic contributions to the shear elastic constants (figures 2 and 3) are very small. It is only approximately valid for the CSDW phases of the other two Cr–Ir crystals, for which magnetic contributions to the shear elastic constants for $T_{IC} < T < T_N$ are a little larger than those for the former two crystals, but still much smaller than the magnetic contributions to the longitudinal mode constants. We analysed the results for the ISDW phases of the Cr + 0.07 at.% Ir and Cr + 0.17 at.% Ir crystals and for the CSDW phases of the two crystals containing 0.20 and 0.25 at.% Ir. Below T_N, but not in the limit $T \to T_N$, the magnetic free energy [1] is written as

$$\Delta F(t, \omega) = \phi(\omega) f(t(\omega)) \tag{1}$$

where $\phi(\omega)$ depends on the volume strain. Here $f(t(\omega))$ is taken [1] as $f(t(\omega)) = (1-t^2)^2$, where the reduced temperature $t = T/T_0(\omega)$, and $T_0(\omega)$ is a critical temperature parameter. It was found, to a good approximation, for Cr–Fe [30] and Cr–Si [11] alloys that T_0 is given by T_N. In analysing the Cr–Ir data we also used this approximation.

It follows [11, 30] from equation (1) that

$$\Delta\omega = a_0 + a_1 t^2 + a_2 t^2 \tag{2}$$

and

$$\Delta B = b_0 + b_1 t^2 + b_2 t^4 \tag{3}$$

where ΔB is the magnetic contribution to B and $\Delta\omega$ is the magnetovolume. The constants (a_0, a_1, a_2) and (b_0, b_1, b_2) contain ϕ, its first and second derivatives (ϕ' and ϕ'') with respect to strain, as well as $\mathrm{d}\ln T_N/\mathrm{d}\omega$. The theory also gives

$$a_1/a_0 + a_2/a_0 = -1. \tag{4}$$

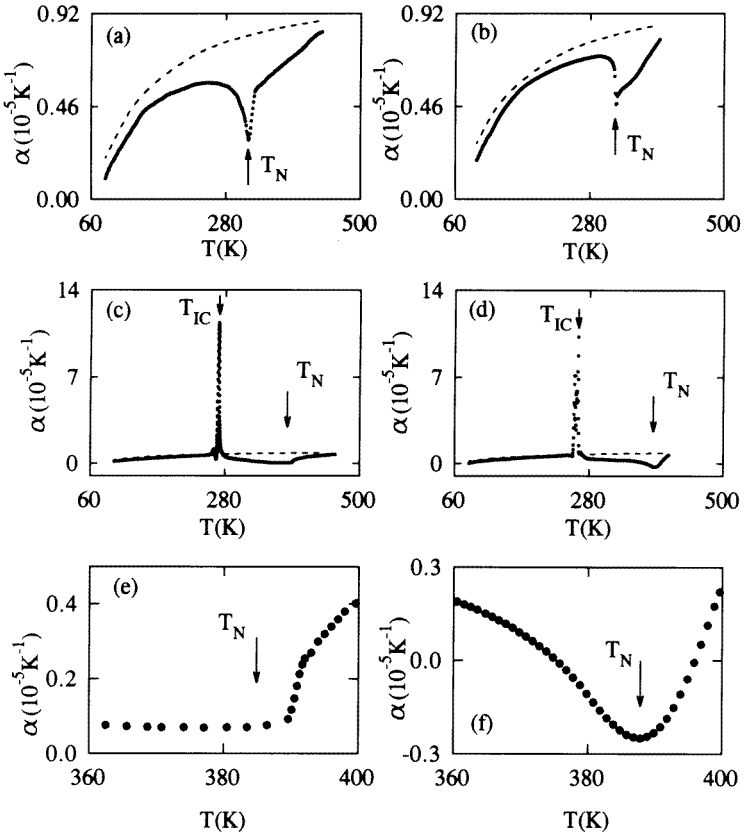

Figure 12. The coefficient of thermal expansion, α, as a function of temperature for (a) Cr+0.07 at.% Ir, (b) Cr + 0.17 at.% Ir, (c) Cr + 0.20 at.% Ir and (d) Cr + 0.25 at.% Ir. Panels (e) and (f) show, respectively, α for Cr + 0.20 at.% Ir and Cr + 0.25 at.% Ir close to T_N. Data are shown for heating runs. The broken lines show the temperature dependence of α for Cr + 5 at.% V. Note the different temperature scales used in the different figures.

Fawcett and Alberts [28, 29] considered ϕ in equation (1) as a constant for the temperature regions $T \rightarrow T_N$ from above or from below. This leads [1] to the following equations for these temperature regions:

$$\frac{\mathrm{d}T_N}{\mathrm{d}\omega} = \frac{1}{B}\lim_{t\to 1}(\Delta B/\Delta\beta) \qquad t < 1 \tag{5}$$

and

$$\frac{\mathrm{d}T_F}{\mathrm{d}\omega} = \frac{1}{B}\lim_{t\to 1}(\Delta B/\Delta\beta) \qquad t > 1. \tag{6}$$

Here T_F is a characteristic spin-fluctuation temperature and $\Delta\beta = 3\,\Delta\alpha$ is the magnetic contribution to the coefficient of volume thermal expansion. The requirement that $\mathrm{d}T_N/\mathrm{d}\omega$ and $\mathrm{d}T_F/\mathrm{d}\omega$ be determined only in the limit $T \rightarrow T_N$ is not stringent [28]. Plots of $\Delta B(t)$ against $\Delta\beta(t)$, both above and below T_N, were found to be linear over a relatively wide temperature range near T_N for several Cr alloy systems [1, 11, 29, 30]. One can then determine the above quantities from these linear parts.

The experimental data for $\Delta\omega$ and ΔB for the Cr–Ir crystals were found to fit equations (2) and (3) very well over a temperature range of about 150 K, or more, below T_N for the ISDW phases of the Cr + 0.07 at.% Ir and Cr + 0.17 at.% Ir crystals and over a range of about 80 K for the CSDW phases, just below T_N, of the other two crystals. The fitting parameters were of the same order of magnitude as that obtained previously for Cr–Si [11] and Cr–Fe [30] alloys. By applying equation (4) to the coefficients obtained in the fits, we found for the left-hand side of equation (4) values of −0.65, −0.45, −0.71 and −0.83 for the Cr–Ir crystals with respectively 0.07, 0.17, 0.20 and 0.25 at.% Ir. These values are similar to values obtained for Cr–Si [11] and Cr–Fe [30] alloys.

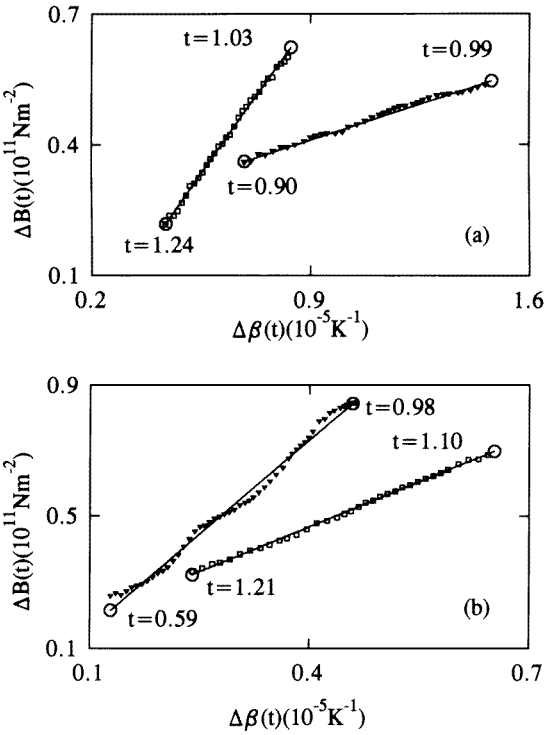

Figure 13. The magnetic contribution to the bulk modulus, $\Delta B(t)$, as a function of the magnetic contribution to the volume thermal expansion coefficient, $\Delta\beta(t)$: (a) Cr + 0.07 at.% Ir and (b) Cr + 0.17 at.% Ir. The straight lines are least-squares fits to the data and the values of t at the encircled points are shown in the figures.

For the two crystals containing 0.07 at.% Ir and 0.17 at.% Ir, which remain in the ISDW phase for all $T < T_N$, we found ΔB to be proportional to $\Delta\beta$ over reasonably large temperature regions both below and above T_N. This is shown in figure 13. We could not find useful linear regions of ΔB versus $\Delta\beta$ for the CSDW phases of the Cr + 0.20 at.% Ir and Cr + 0.25 at.% Ir crystals. We obtain from equations (5) and (6) and the slopes of figures 13(a) and 13(b) $\mathrm{d}T_N/\mathrm{d}\omega = 0.13 \times 10^5$ K and 1.27×10^5 K, respectively, for $T < T_N$ for the Cr + 0.07 at.% Ir and Cr + 0.17 at.% Ir crystals. These values are to be compared with $\mathrm{d}T_N/\mathrm{d}\omega$ obtained from direct high-pressure measurements of $\mathrm{d}T_N/\mathrm{d}p$. Unfortunately $\mathrm{d}T_N/\mathrm{d}p$ was only measured up to now for the former crystal, giving [23]

$dT_N/dp = -58 \pm 4$ K GPa^{-1}. From this value we obtain, using the equation [31]

$$dT_N/d\omega = -B(dT_N/dp)[1 - 3\alpha B\ dT_N/dp]^{-1}. \tag{7}$$

$dT_N/d\omega = (0.18 \pm 0.02) \times 10^5$ K, which compares reasonably well with the value obtained from figure 13 for the Cr + 0.07 at.% Ir crystal. The error in $dT_N/d\omega$ obtained from figure 13 is estimated to be between 10% and 20%.

For $T > T_N$ we obtain from figure 13 $dT_F/d\omega = 0.58 \times 10^5$ K and $dT_F/d\omega = 0.60 \times 10^5$ K, respectively, for Cr + 0.07 at.% Ir and Cr + 0.17 at.% Ir. In the former crystal $dT_F/d\omega > dT_N/d\omega$, as was also observed for other dilute Cr alloys [11, 28]. This means that the short-range magnetic order and spin fluctuations above T_N in the Cr + 0.07 at.% Ir crystal are more volume dependent than the SDW below T_N. In the Cr + 0.17 at.% Ir crystal the situation is however just the reverse; $dT_F/d\omega < dT_N/d\omega$. This is the only Cr alloy of which we are aware for which $dT_F/d\omega < dT_N/d\omega$. It must however be kept in mind that the Cr + 0.17 at.% Ir sample is very close to the triple-point Ir concentration of 0.15 at.% Ir [20]. We suggest that this fact possibly makes T_N for this crystal very unstable against volume changes, a fact that is to be verified by direct dT_N/dp measurements. The Cr + 0.17 at.% Ir crystal behaves also anomalously in its magnetovolume. At low temperatures, where all four Cr–Ir crystals are in the ISDW phase, $|\Delta\omega| \approx 1 \times 10^{-3}$ for Cr + 0.17 at.% Ir while for the other three crystals $|\Delta\omega| \approx 2 \times 10^{-3}$.

Sato and Maki [32] studied the ultrasonic attenuation of dilute Cr alloys above T_N theoretically. They found that γ for both longitudinal and shear waves should diverge as $(T/T_N - 1)^{-1/2}$ for a transition into the ISDW state, no divergence for a transition into the CSDW state and a divergence as $(T/T_N - 1)^{-5/4}$ for an alloy with a concentration in the vicinity of the triple-point concentration. Our data for γ for Cr + 0.07 at.% Ir (figure 9(a)) could not be fitted for $T > T_N$ to the power law $(T/T_N - 1)^{-1/2}$. On the other hand, γ for the c' mode of the Cr + 0.17 at.% Ir crystal, which is close to the triple-point concentration, fits the power law $(T/T_N - 1)^{-5/4}$ predicted by Sato and Maki [32] very well for temperatures just above T_N. Due to the fact that we could not measure γ successfully near T_N for the Cr + 0.20 at.% Ir and Cr + 0.25 at.% Ir crystals, we could not test Sato and Maki's [32] results for the transition into the CSDW phase.

Katsnel'son and Trefilov [33] recently studied the anomalies in the elastic constants and thermal expansion of Cr alloys theoretically. They considered the effects of the disappearance of the antiferromagnetic SDW energy gap in the electron spectrum on the electron screening and phonon spectrum of the alloys, and showed that the elastic constants should soften and that there is a negative contribution to the thermal expansion coefficient at T_N. The theory further predicts that B should soften much more than the shear elastic constants. These predictions of the theory are fulfilled by the present study on Cr–Ir alloys, as is also the case for other dilute Cr alloys [1]. Katsnel'son and Trefilov [33] found that the magnetic contributions to the thermal expansion and shear elastic constants should vary as $(T_N - T)^{-1}$ if the density-of-states function in the paramagnetic phase is smooth near the Fermi level and as $(T_N - T)^{-5/4}$ if it has a van Hove singularity there. The results of the present study on Cr–Ir alloys were however found not to fit any one of these two power laws.

5. Conclusions

The magnetoelastic properties of dilute Cr–Ir alloy single crystals were studied for the first time for alloys containing 0.07, 0.17, 0.20 and 0.25 at.% Ir. All elastic constants soften when the spin-density-wave state is entered on cooling through the Néel transition. The softening

of the longitudinal mode constants is the largest, up to 35%, while it is only about 3% for the shear mode constants. This observation shows that the Cr–Ir crystals very closely fulfil the assumptions of the thermodynamic model for the magnetoelasticity of dilute Cr alloys, making the model applicable for analysing the temperature dependence of the magnetic contributions to the bulk modulus (ΔB) and the magnetovolume ($\Delta\omega$) of the Cr–Ir system. The model successfully fits $\Delta B(T)$ and $\Delta\omega(T)$ for the incommensurate spin-density-wave states of the two alloys containing 0.07 and 0.17 at.% Ir as well as for the commensurate spin-density-wave states of the two containing 0.20 and 0.25 at.% Ir. It also gives a value of the volume derivative of the Néel temperature of the Cr + 0.07 at.% Ir crystal, calculated from the magnetic contributions to the bulk modulus and thermal expansion, that agrees fairly well with a value obtained from direct high-pressure measurements. The suitability of the thermodynamic model for analysing the magnetoelastic properties of dilute Cr alloys is now well established. The longitudinal elastic constants of the Cr+0.20 at.% Ir and Cr+0.25 at.% Ir crystals stiffen by about 6% and the shear constants by about 3% when they are cooled through the commensurate–incommensurate (C–I) spin-density-wave transition. This transition is hysteretic with a hysteresis width of about 20 K, very similar to that observed previously for a Cr + 0.3 at.% Ru alloy which is also a member of the Cr alloy system with group-8 non-magnetic transition metals. The ultrasonic attenuation coefficient (γ) of the Cr–Ir alloy crystals shows well defined peaks at the spin-flip transition temperature as well is at the C–I and I–C transition temperatures. Peaks were also observed in $\gamma(T)$ for Cr + 0.07 at.% Ir and Cr + 0.17 at.% Ir at the Néel transition. We were not able to measure $\gamma(T)$ for the other two crystals.

Acknowledgment

Financial aid from the South African Foundation for Research Development is acknowledged.

References

[1] Fawcett E, Alberts H L, Galkin V Yu, Noakes D R and Yakhmi J V 1994 *Rev. Mod. Phys.* **66** 25
[2] Cankurtaran M, Saunders G A, Sidek H A A, Wang Q and Alberts H L 1996 *Phys. Rev.* B **53** 11 408
[3] Alberts H L and Smit P 1995 *J. Magn. Magn. Mater.* **140–144** 41
[4] Alberts H L and Lourens J A J 1988 *J. Physique.* **49** C8 215
[5] Munday B C 1971 *Phys. Status Solidi* a **8** K129
[6] Alberts H L and Lourens J A J 1988 *J. Phys. F: Met. Phys.* **18** L213
[7] Alberts H L and Boshoff A H 1992 *J. Magn. Magn. Mater.* **104–107** 2031
[8] Cankurtaran M, Saunders G A, Wang Q, Ford P J and Alberts H L 1992 *Phys. Rev.* B **46** 14 370
[9] Boshoff A H, Alberts H L, du Plessis P de V and Venter A M 1993 *J. Phys.: Condens. Matter* **5** 5353
[10] Martynova J, Alberts H L and Smit P 1996 *J. Appl. Phys.* **79** 6519
[11] Anderson R A, Alberts H L and Smit P 1993 *J. Phys.: Condens. Matter* **5** 1733
[12] Waterstrat R M and Manuszewski R C 1973 *J. Less-Common Met.* **32** 79
[13] Bohlmann M and Alberts H L 1970 *J. Phys. E: Sci. Instrum.* **3** 779
[14] Papadakis E P 1976 *Physical Acoustics* vol xii, ed W P Mason and R N Thurston (New York: Academic)
[15] Alberts H L and Lourens J A J 1984 *Phys. Rev.* B **29** 5279
[16] Truell R, Elbaum C and Chick B B 1969 *Ultrasonic Methods in Solid State Physics* (New York: Academic)
[17] Kittinger E 1977 *Ultrasonics* **15** 30
[18] Alberts H L 1990 *J. Phys.: Condens. Matter* **2** 9707
[19] Martynova J, Alberts H L and Smit P 1996 *J. Phys.: Condens. Matter* **8** 10 473
[20] Butylenko A K and Nevdacha V V 1980 *Dokl. Akad. Nauk. Ukr. SSR* A **5** 67 (in Russian)
[21] de Camargo P C, Fawcett E and Perz J M 1990 *J. Appl. Phys.* **67** 5265
[22] Eccleston R S, Hagen M, Mañosa Ll, Saunders G A and Alberts H L 1996 *J. Phys.: Condens Matter* **8** 7837

[23] Martynova J, Alberts H L and Smit P 1996 *J. Phys.: Condens. Matter* **8** 4045
[24] Werner S A, Arrott A and Kendrick H 1967 *Phys. Rev.* **155** 528
[25] Kondorsky E I, Kostina T I, Medvedchikov V P and Popova N N 1978 *Fiz. Met. Metalloved.* **45** 1317 (in Russian)
[26] Kostina T I, Galkin V Yu, Kondorsky E I and Katerinchuk A V 1975 *Fiz. Met. Metalloved.* **40** 851 (in Russian)
[27] Roberts R B, White G K and Fawcett E 1983 *Physica* B **119** 63
Roberts R B, White G K and Fawcett E 1983 private communication
[28] Fawcett E and Alberts H L 1990 *J. Phys.: Condens. Matter* **2** 6251
[29] Fawcett E and Alberts H L 1992 *J. Phys.: Condens. Matter* **4** 613
[30] Alberts H L and Lourens J A J 1992 *J. Phys.: Condens. Matter* **4** 3835
[31] Bloch D and Pavlovic H A 1969 *Advances in High Pressure Research* (New York: Academic)
[32] Sato H and Maki K 1973 *Int. J. Magn.* **4** 163
[33] Katsnel'son M I and Trefilov A V 1994 *Phys. Met. Metallogr.* **77** 362